



OPEN

## Combination of US hyperthermia and radiotherapy on a preclinical glioblastoma model

Gianni Durando<sup>1,4</sup>, Federica Vurro<sup>2,4</sup>, Fabio Saba<sup>1</sup>, Aoife M. Ivory<sup>3</sup>,  
Raphaella de Melo Baesso<sup>3</sup>, Piero Miloro<sup>3</sup> & Antonello E. Spinelli<sup>1</sup>

In this work the effect of combining ultrasound (US) hyperthermia (HT) with radiotherapy (RT) was investigated. The treatment was applied to a GBM xenograft nude mouse model obtained by injecting  $2 \times 10^6$  U87 luc+ cells. The combined treatment group received 6 Gy and HT at 43 °C for 8 min. The ultrasound field was generated by a closed-loop computationally controlled system, consisting of a High Intensity Focused Ultrasound (HIFU) transducer with centre frequency 3.57 MHz, a power amplifier, a function generator and a MATLAB controller. A mechanical cone adaptor has been designed to use the HIFU beam at a pre-defined post-focal distance. Two thermocouples were placed between the mechanical cone and the mice skin to measure and control the temperature during the HT treatment. Radiotherapy was carried out by using a dedicated small animal image guided radiotherapy system. Measurements of tumor volume performed with a caliper showed good tumor control for the RT-HT group with respect to the RT or control groups for up to 21 days after treatment. The mean value of the normalized (before therapy) tumor volume was almost equal to 0.5 for two weeks after treatment with an increase to 1.5 at sacrifice. The control and HT groups showed a higher value of about 1.5 during the first two weeks and 3.5 at the end of the follow-up period. We concluded that the use of HT as a radiosensitizer can improve the outcome for glioblastoma treatments.

Glioblastoma (GBM) is one of the most aggressive brain tumors, with a short life expectancy and an elevated mortality because of the lack of effective therapies. The median survival of is equal to 15 months months after diagnosis<sup>1</sup>. GBM is resistant to conventional radiotherapy (RT) and, thus, innovative approaches must be developed to improve the therapeutic outcomes. Hyperthermia (HT) has been shown in the past to be a potential radiosensitizer<sup>2</sup>. In this work, the use of HT in combination with RT was investigated in vivo on a preclinical GBM model. The biological mechanisms behind the effects of HT in combination with RT are not fully understood, the main hypothesis assumes a limited ability of the cells to cope with radiation-induced DNA damage when heated<sup>3</sup>. The main parameters describing HT treatments are the temperature  $T$  and the heating time  $t$ . To compare different heating schemes, an index called Cumulative Equivalent Minutes (CEM) at 43 °C is defined as follows:

$$CEM_{43^\circ C} = \int_0^t R^{(43-T)} dt \quad (1)$$

where  $R$  is a constant equal to 0.5 if  $T > 43^\circ C$  or 0.5 if  $T < 43^\circ C$ <sup>4</sup>. Another important parameter that needs to be considered when combining HT and RT is the time between the two treatments. While there is no agreement on the ideal treatment approach (e.g. HT then RT or vice versa), there is a consensus that the shorter the time between the two, the better the outcome<sup>3</sup>. HT can be delivered in vivo using different approaches like photothermal therapy, electromagnetic fields (microwaves and radio waves), and ultrasound (US)<sup>5</sup>. Gold nanoparticles (GNPs) can be used to obtain selective heating in deeper body regions thanks to the GNP absorption of light in the near-infrared (NIR) region. In this case, NIR light, typically produced by a laser, can penetrate tissues with sufficient intensity for inducing localized hyperthermia<sup>6</sup>. Another common approach to deliver HT is the use of microwaves and radio waves with frequencies ranging between 70 to 1000 MHz. The penetration depth decreases with increasing frequency and in general wet tissues (e.g. muscle) absorb more energy than dry tissues

<sup>1</sup>National Institute of Metrological Research (INRIM), Strada delle Cacce 91, 10135 Turin, Italy. <sup>2</sup>Experimental Imaging Centre, IRCCS San Raffaele Scientific Institute, Via Olgettina 60, 20132 Milan, Italy. <sup>3</sup>National Physical Laboratory, Teddington, UK. <sup>4</sup>These authors contributed equally: Gianni Durando and Federica Vurro. email: spinelli.antonello@hsr.it

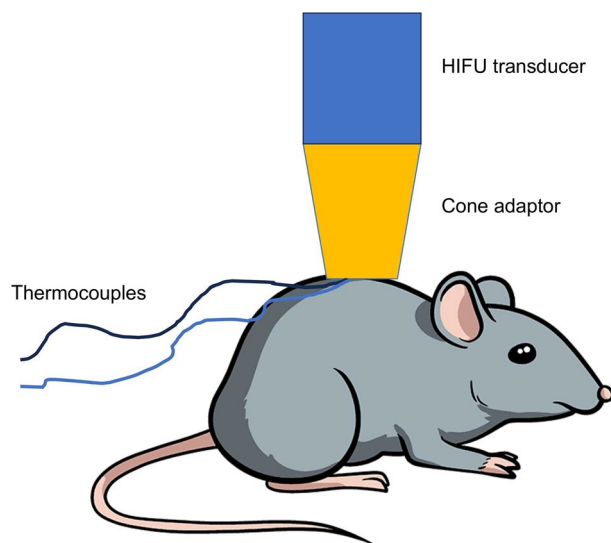


**Figure 1.** An example of the US transducer positioning (hand-guided) during in vivo HT treatment.

(e.g. fat)<sup>7</sup>. These systems are thus designed to deliver superficial hyperthermia, i.e. heating tumors extending to depths less than 3 - 4 cm, and loco-regional or deep hyperthermia, i.e. heating tumors at depths larger than 4 cm or situated centrally in the body.

In this work the use of US to deliver HT on small animals was investigated. A custom-developed US-based preclinical hyperthermia system was used to uniformly heat a superficial area of about 1 cm diameter. Using this setup, it was possible to heat the entire mouse tumor volume without the need to move the animal and, thus, reducing the time (less than 1 min) between RT and HT. The system, described and characterized in a previous work<sup>8</sup> and briefly presented in the materials and methods, is based on a custom-designed cone attached to an HIFU probe. The main feature of the cone is to spread the US beam across a relatively large superficial area resulting in the ability to perform HT on the whole mouse tumor at the same time. The compact preclinical HT tool was installed next to a state-of-the-art image-guided small animal irradiator with a dedicated Monte Carlo dose planning system. Using this experimental set-up it was possible to deliver RT dose, to reduce the time between RT and HT, and to achieve a constant temperature on the tumor during the entire HT treatment. The outcome of the combined RT-HT treatments was investigated in vivo with a xenograft GBM model and evaluated by following the tumor progression using volume measurements and bioluminescence imaging for up to 3 weeks after the treatments. Ex vivo analysis of the tumor tissue was also performed as described in the materials and methods, discussion and conclusion then followed.

## Results

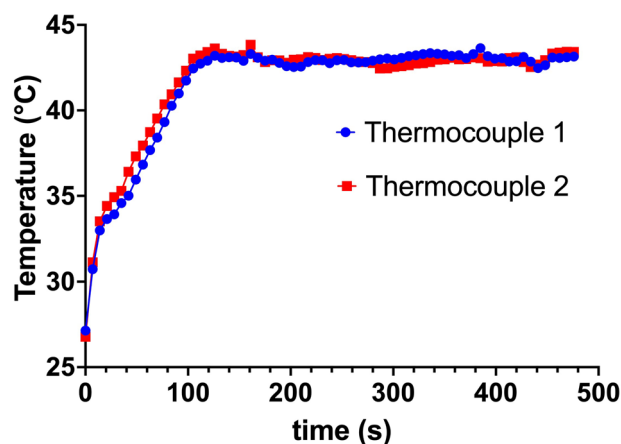
### In vivo hyperthermia measurements

Figure 1 shows the use of the transducer during in vivo experiments. The system allowed control of the exposure based on temperature measured within adjustable limits, increasing or decreasing the delivered voltage to the transducer depending on the measured voltage compared to these limits. For all exposures present here, the target temperature was 43 °C, which is generally accepted to be the target for hyperthermia treatments. An example of the monitored temperature during the experiment is shown in Fig. 2.

### Tumor growth measurements

As can be seen in Fig. 3, the measurements of tumor volume show good tumor control for the RT-HT group with respect to the RT or control groups for up to 21 days after treatment. More precisely, the mean value of the normalized tumor volume was almost constantly equal to 0.5 for two weeks after treatment with an increase to 1.5 at sacrifice. On the other hand, the other groups showed a higher value of about 1.5 during the first two weeks and 3.5 at the end of the follow-up period. As mentioned in the material and methods a statistical analysis between the RT and RT-HT groups has been performed using the Mann-Whitney test. A statistically significant difference ( $p < 0.05$ ) has been found from ten days after treatment.

Figure 4 shows the measured BLI signal of the tumor region at different time points up to 21 days after treatment. The BLI signal of the RT-HT group is stable and lower with respect to the RT or control groups for all three weeks after treatment. Interestingly the BLI signal rapidly increased for the control group after 21 days, almost doubling with respect to day 3, while as expected the RT group lies between the control and RT-HT groups. The BLI data are also in agreement with the volume measurements presented in Fig. 3. A statistically significant difference ( $p < 0.05$ ) has been found for day 7 and 14 after treatment.



**Figure 2.** The plot shows an example of measured temperatures during the in vivo HT delivery.

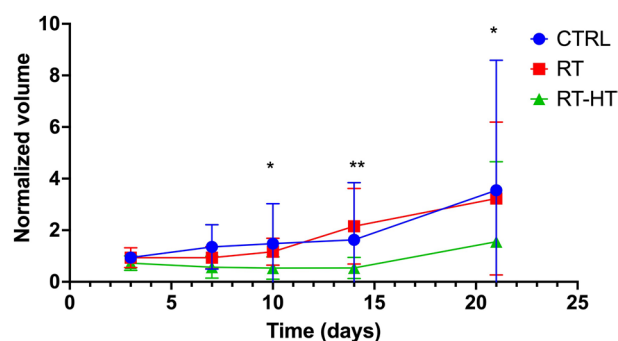


**Figure 3.** The plot shows the normalized tumor volume measured at different time points after treatment. Statistical analysis between the RT and RT-HT groups has been performed using the Mann–Whitney test. A statistically significant difference ( $p < 0.05$ ) has been found from ten days after treatment.

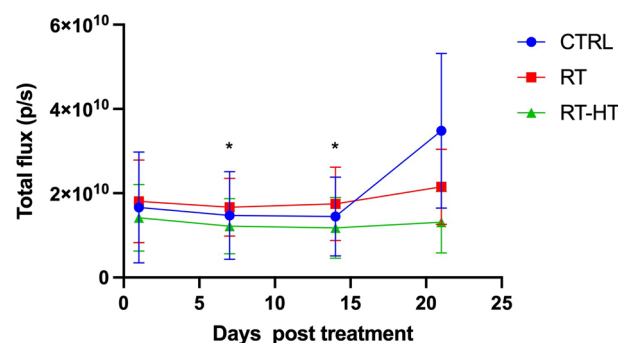


**Figure 4.** The plot shows the total flux photons/seconds (p/s) values of a ROI placed over the tumor. Bioluminescence imaging was performed at different time points. A statistically significant difference ( $p < 0.05$ ) has been found for day 7 and 14 after treatment.

### Ex vivo analysis

IHC analyses were performed on tumor tissue dissected out 21 days after treatment and showed a lower presence of Ki-67 -positive cells in mice treated with radiotherapy and hyperthermia as compared to control group and radiotherapy group (Fig. 5) confirming data obtained analyzing tumor growth. To gain insight into the mechanism of cell death, after Hyperthermia, tumors were processed for an immunohistochemical protocol to evaluate the expression of HSP70, selected as an indicator of cellular stress, including temperature increase. Since the mice were euthanized three weeks after hyperthermia and radiotherapy treatment, we could not observe a difference in HSP70 expression in tumor tissues, whose expression is characterized by a peak at 12 h<sup>9</sup>.

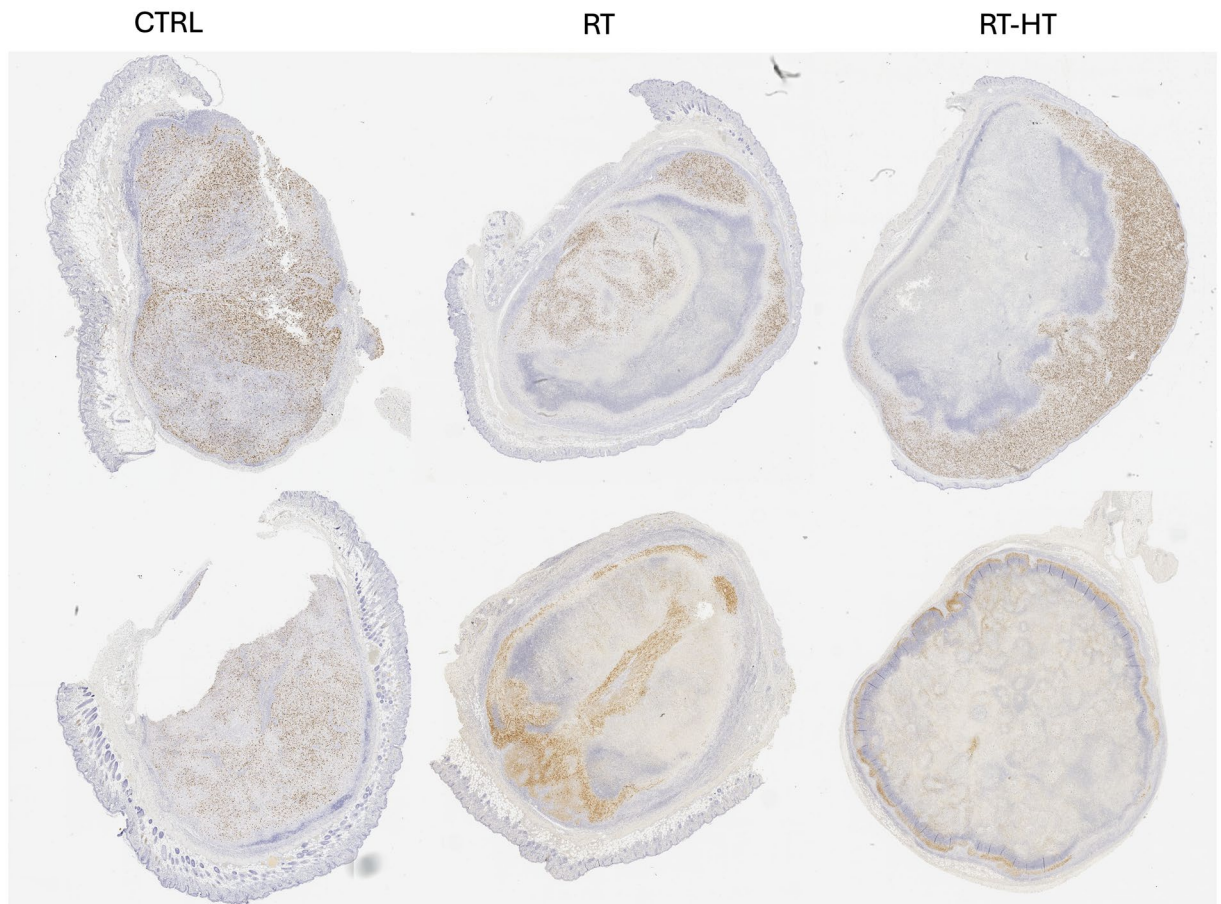


**Figure 5.** Immunohistochemical analysis show that Ki67 expression is higher in the untreated tumor (CTRL) and in the tumor treated with radiotherapy (RT) in comparison to the one treated with radiotherapy and hyperthermia (RT-HT).

## Discussion

The use of HT in combination with RT has the potential advantage of increasing the local tumor control without increasing the treatment dose. To fully exploit the HT radiosensitizing effect it is necessary to reduce the time between the two treatments and, at the same time, to achieve an adequate CEM value over the entire tumor volume. In this paper, the effect of HT delivered using US immediately after RT was investigated using a preclinical xenograft GBM model. The combination of HT and RT on GBM was studied as it is a radio-resistant tumor and, thus, the use of HT as a radiosensitizer might significantly enhance the radiotherapy outcome of GBM treatments. Using our prototype, we were able to rapidly increase locally (in the tumor region) the temperature in the range of 42–45 °C. The temperature increase was obtained in a measurable (real-time) and controlled way for a few minutes. Other approaches might be employed to perform HT, using for example nano particles or electromagnetic fields, however the temperature control and the time of HT delivery is typically less reproducible. A protocol was developed based on a closed-loop feedback circuit to maintain the temperature of the treated region at the set point of 43 °C during all HT delivery. This has been achieved by a dedicated MATLAB code that used the temperature measured by two thermocouples to adjust the voltage, in real time. After a transient warm up time of about 100 seconds, it was possible to keep the temperature stable at the set point for the entire duration of the HT treatment, as shown in the results. A potential limitation of using thermocouples is the sampling point (placed on the mouse skin) that might not represent the true temperature inside the tumor. This limitation is however relatively minor for superficial tumors. Other tumor temperature measurement approaches could be used, for example, based on Magnetic resonance imaging (MRI), however, such approach could not be performed with our prototype since, as this development stage, is not MRI compatible. Secondly, MRI thermometry can increase the time delay between RT and HT possibly reducing the efficacy of the combined treatment. In summary, despite the limitations mentioned above, the temperature measurement approach based on thermocouples was considered a good practical solution to monitor and adjust in real-time, the temperature while also reducing the time between RT and HT treatment. In vivo, results obtained by monitoring tumor growth with a caliper and with BLI show better tumor control for the RT-HT group with respect to RT alone for up to 21 days after treatment. The standard deviation in Figs. 4 and 5 show that the values, in particular for the control group, are quite scattered however the trend for the RT-HT group was always better, even using the moderately low radiotherapy dose of 6



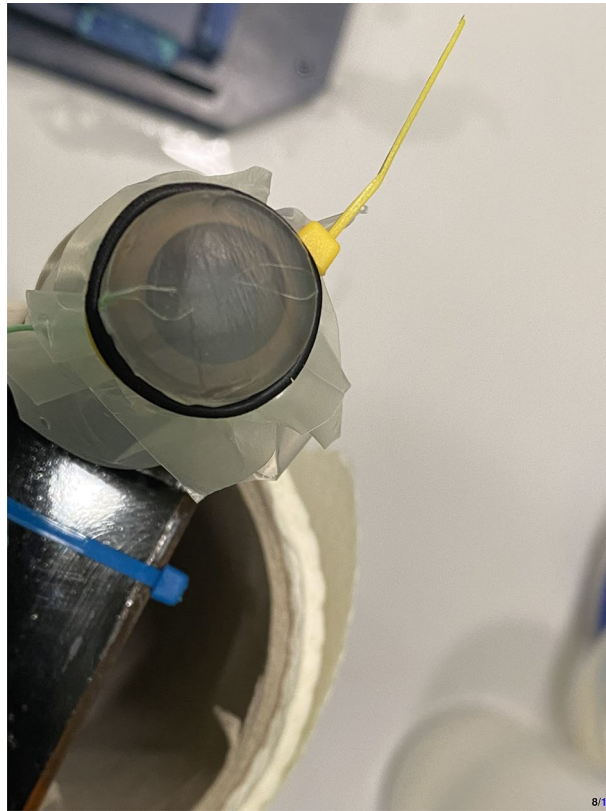


**Figure 6.** Two thermocouples were used to record the temperature throughout for the temperature control during the in vivo experiments.

Gy. A statistically significant difference has been found from ten days after treatment. These data showed that HT delivered using the proposed US preclinical system was acting as a radiosensitizer in the preclinical GBM model.

IHC analysis was performed on tumor tissue to study the expression of Ki67 and HSP70 after the treatment. Ki-67 is a nuclear protein, and it reflects the proliferative state of the cells in which this marker is expressed. In this way, Ki67 may be a potent tool for easy and quick evaluation of the proportion of proliferating cells in a tumor. The immunohistochemical analysis performed on tumor tissue showed a lower expression of Ki-67 in mice treated with radiotherapy and hyperthermia when compared to both the control group and the radiotherapy group, supporting data obtained analyzing tumor growth (which showed a better tumor control for the RT-HT group with respect to RT alone for up to 21 days after treatment). Since the main goal of the paper was to evaluate the tumor response of the combined HT-RT (with respect to RT or untreated) to reduce the number of mice used we decided to perform the ex vivo analysis only at the end of the experiment, without sacrificing any animal at intermediate time points. Using this experimental protocol, we couldn't observe a difference in HSP70 expression on tumor tissue of different groups. The reason we could not see a difference between the groups may be due to the late timing of the euthanasia<sup>9</sup>.

With regard to future work the main problems we'll be facing in translating our findings into a clinical setting are an accurate temperature measurement and a homogenous heating across the tumor region. The HT system should be also compact and lightweight in order to be moved in and out of a radiotherapy bunker to reduce the time between HT and RT. The next steps are thus focused on developing a system similar to<sup>10</sup> in order to have US guidance for HT delivery with a broader US beam to cover the tumor region.

## Methods

### Materials and methods

#### Hyperthermia ultrasound system

The ultrasound field was generated by a High-Intensity Focused Ultrasound (HIFU), transducer (Sonic Concepts, SU-103) driven in continuous wave mode at the center frequency of 3.57 MHz by a function generator (Agilent 33220A) connected to a 55 dB power amplifier (Amplifier Research 150A100D). A mechanical cone adaptor was developed to use the HIFU far field as shown in Fig. 6. Two thermocouples were placed between the mechanical cone and the mouse skin to measure and control the temperature during the HT treatment. The voltage delivered to the system was controlled via closed-loop feedback to the function generator via a MATLAB interface (R2019a, MATLAB, The Mathworks, USA). There were 2 K-type 75  $\mu$ m diameter thermocouples (5SRTC-TT-KI-40-1M, Omega, USA). A thermocouple data logger (Pico USB TC 08, PicoTechnology, UK) read the temperature from the 2 thermocouples throughout the treatment. The target temperature was set within the MATLAB code to

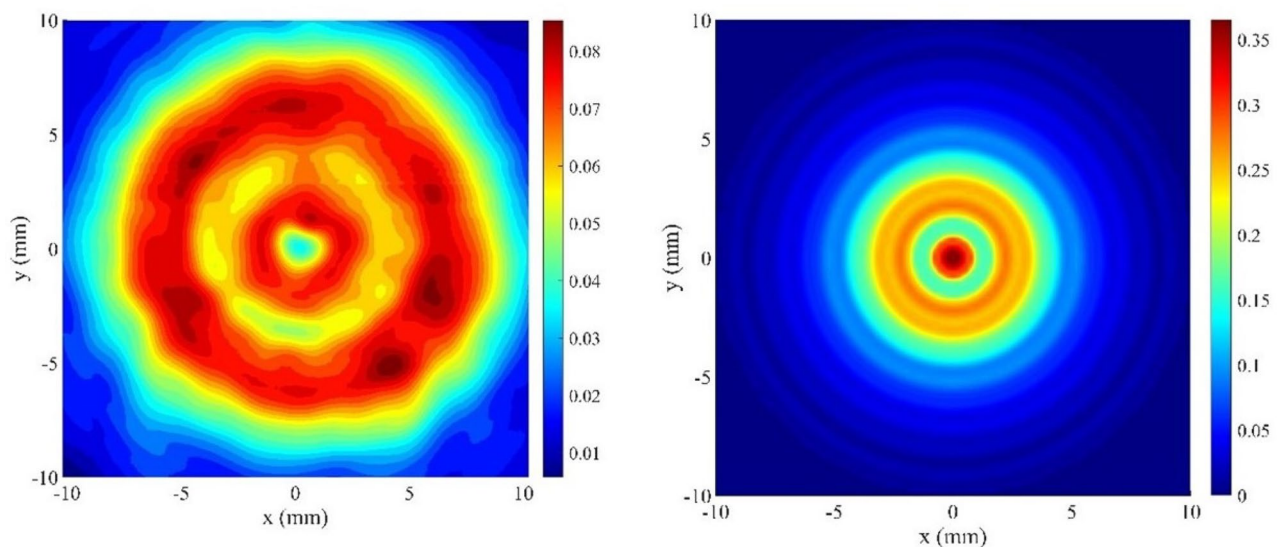


**Figure 7.** Peak positive pressure in MPa from the transducer, measured 30 mm from the focus, with the cone in place, and projected 15 mm from the focus, where the exposure was performed. For the measurements, the output power of the transducer was set at 4.2 W.

43.0 °C and the upper and lower limits around this temperature were set as  $T_{high}$  (43.5 °C) and  $T_{low}$  (42.5 °C), respectively. When the temperatures were read across the 2 thermocouples, the highest thermocouple temperature was compared to these values; the temperature control started after an initial period of about 30 seconds, in which the voltage output from the function generator was kept constant, subsequently, the voltage delivered to the transducer was slowly increased until the target temperature was reached. Then, to keep the temperature within the control range, the voltage was adjusted, if the temperature was above  $T_{high}$ , the voltage output from the function generator was decreased, if the temperature was lower than  $T_{low}$ , it was increased. The temperature was queried every 7 seconds for 8 minutes, first to achieve heating in the target region and then to maintain the temperature within the acceptable range. Output voltages from the function generator and the temperature measured by the thermocouples were recorded at each time point. The bench-level hyperthermia delivery system was fully characterized and tested<sup>8</sup>. The system was tested on a thermochromic tissue mimicking material, showing the ability to raise the temperature only in the target area, with negligible effects on the surrounding material. For completeness, in Fig. 7 we show the field measured 30 mm after the focus, with the cone in place, and the projected field 15 mm after the focus, where the exposure was performed. As expected, the radiated power increases approximately quadratically with the drive voltage.

### Small animal radiotherapy

Radiotherapy dose was delivered using a dedicated small animal micro-irradiator with micro cone beam computed tomography (CBCT) guidance<sup>11</sup>. The small animal micro-irradiator (X-RAD225Cx SMART, PXI North Branford, CT, USA) is based on a 225 kVp x-ray tube (Comet MXR-225/22 tube, GE Isovolt 225 Titan generator) and an amorphous silicon (1024 × 1024) x-ray panel detector (PerkinElmer). Both the x-ray tube and flat panel detector are mounted on a C-arm gantry that can rotate 360°, the object is placed at the center of rotation and is stationary during both imaging and treatment. Mice were anesthetized with gaseous anesthesia (2–3% isoflurane and 1 l/min oxygen). The anesthetized mice were positioned prone on the animal stage and underwent the entire treatment, mimicking the radiotherapy workflow. CBCT images were acquired for treatment planning using the following settings: tube voltage=40 kVp, current= 5 mA, voxel size=0.1 mm<sup>3</sup>. The tumor was contoured using the CBCT dataset and two equal-sized treatment beams were set at 180° and 0° angles respectively as shown in Fig. 8. The field size at the isocenter was equal to: 10 × 10 mm<sup>2</sup>. The dose distribution in the tumor was calculated using a Monte Carlo-based treatment planning system (SmART-ATP)<sup>12</sup> and the mean dose to the tumor was adjusted to the prescribed dose of 6 Gy and delivered in a single fraction. The SmART-ATP treatment planning system allow also to calculate the dose volume histogram (DVH) of the tumor as shown in Fig. 8. The irradiation settings were: tube voltage = 225 kVp and current = 13 mA. Delivery time was about 40 seconds/field, and the entire procedure (CT imaging + RT) was performed within 20 min.

### Bioluminescence imaging

Bioluminescence imaging (BLI) was performed before and after the treatments to monitor the tumor growth. BLI was performed by using the IVIS SpectrumCT System (Perkin Elmer, USA). The system is composed of a low noise, back-thinned, back-illuminated CCD camera cooled at -90°C with a quantum efficiency in the visible range above 85%. Each mouse received an intra-peritoneal injection of 150 mg luciferin/kg body weight 10 minutes before BLI. During image acquisition, the animals were kept at 37°C and under gaseous anesthesia (2–3% isoflurane and 1 l/min oxygen). Dynamic BLI was performed by acquiring a set of images every 2 minutes from 10 to 20 minutes after luciferin injection to detect the highest BLI signal. The images were obtained using

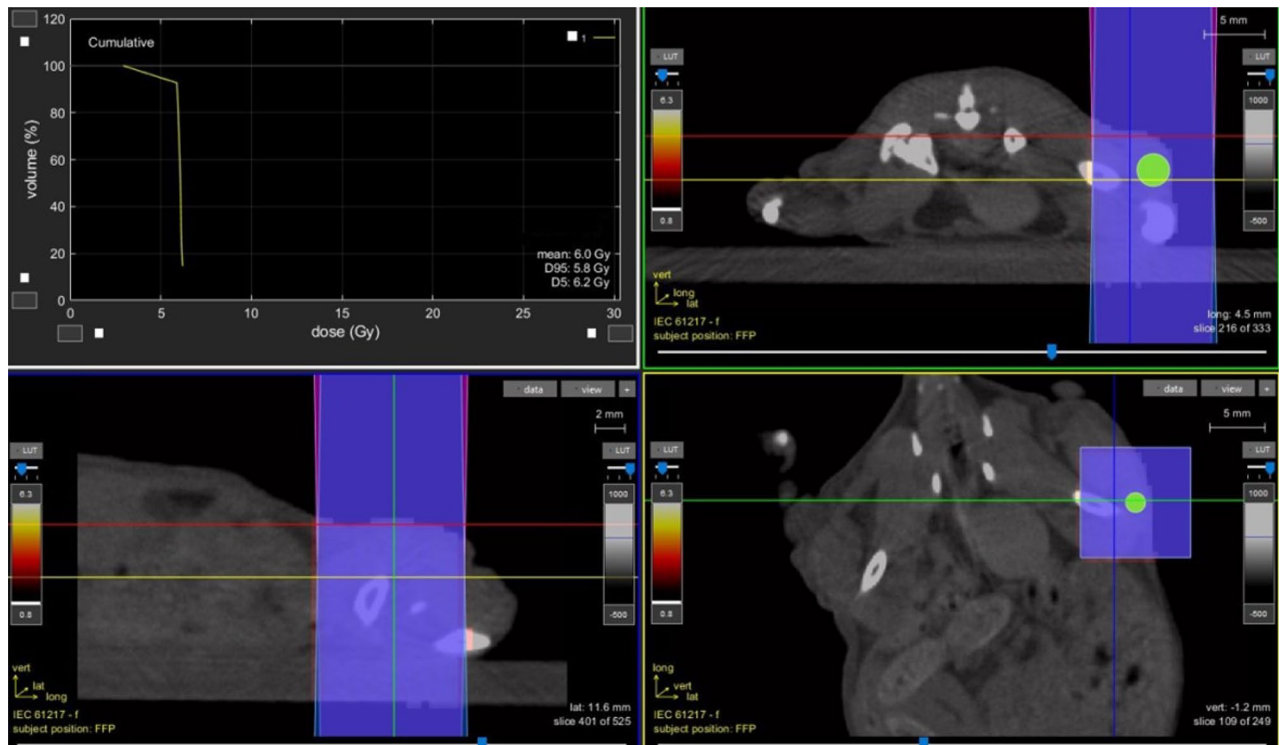


**Figure 8.** The image shows the two beams setup and dose distribution calculated using a Monte Carlo-based treatment planning system (SmART-ATP). The dose volume histogram is shown on the top left box.

the following IVIS settings: exposure time = auto, binning = 8,  $f = 1$ , and a field of view equal to 22 cm (field D). No image emission filters were used during BLI acquisitions. BLI image analysis was performed by placing the Region of interest (ROI) over the tumor and by measuring the total flux (photons/seconds) within the ROI. Images were acquired and analyzed using Living Image 4.5 (Perkin Elmer).

### Glioblastoma preclinical mouse model

The U87 luc+ cell line was cultured in DMEM with 10% (v/v) FBS, 1% (w/v) Gln, 0.5% (v/v) AmpB, 100 units/mL of PS, at 37 °C in a 5% CO<sub>2</sub> humidified atmosphere. Mice were maintained under standard environmental conditions (temperature, humidity, and 12 h/12 h light/dark cycle, with water and food ad libitum) and veterinary control, in the animal facility. Cells were trypsinized when subconfluent (about 80%) and two million cells were injected subcutaneously into the left flank of each mouse (weight 17 - 23 g) to study the effect of the combination of HT and RT on the tumor growth. The size of the tumor was measured daily starting from seven days post-inoculation. After 15 days (when tumor volume reached about 100 mm<sup>3</sup>), the mice were randomly divided into three different treatment groups ( $n = 11$ ). The first group (Control group) was monitored with the caliper to evaluate the tumor growth, the second group was treated with radiotherapy (6 Gy), and the third group received a combination of RT 6 Gy and HT 43° for 8 min. The HT treatment was delivered 1 minute after RT. Tumor size in all mice was measured by caliper at 3, 7, 10, 14, and 21 days post treatment. Individual animal body weight and clinical signs (spontaneous movement, head posture, and social behavior) were monitored. The experimental plan received authorization from the Italian Ministry of Health and was approved by the San Raffaele Scientific Institute ethical committee. Animal experiments were conducted in full compliance with Italian law (D.L. 4 March 2014 no. 26) and European Union regulations (2010/63/EU). This study is reported in accordance with ARRIVE guidelines.

### Ex vivo analysis

For histology, the mice were sacrificed 21 days after hyperthermia and radiotherapy treatment and tumors were dissected out, washed with PBS 0.1 M and fixed in 10% formalin for 4 hours. Tissues were embedded in paraffin, cut in 5 µm thick sections with a microtome and dried at 37 °C for 24 h. To evaluate tissue morphology, sections were stained with Hematoxylin and Eosin. Sections were examined under a light microscope equipped with a charge-coupled device camera. For immunohistochemistry animals were euthanized 21 days post-irradiation, tumors were dissected out, and prepared in the same way as above. The paraffin blocks of OSCC tissue were divided into 6-micron-thick sections. Slides with coatings were used for tissue sections. Deparaffinization is followed by rehydration using different concentrations of alcohol and water. Antigen retrieval was carried out using a 0.01 M citric acid buffer (pH=6.0) heated in the microwave for ten minutes. Following a 15-min incubation in methanol that contained 3% H<sub>2</sub>O<sub>2</sub> to inactivate endogenous peroxidase, slices were then washed with distilled water. Using a rabbit and rat polyclonal antibody against humans and a primary antibody to HSP70 (Ab HSP70 (6B3) Rat mAb N 4873) and Ki67 (Ab Ki-67 (D2H10) Rabbit mAb n 9027); Cell Signaling, Danvers, MA, USA),

the slides were incubated at 4 °C for an overnight period. Immuno-histochemical analysis of tumor tissue sections labeling HSP70 and Ki67 were performed with ab dilution 1:200. Immunoreaction was carried out using the streptavidin-biotin complex method and overnight incubation. Leica BOND RX autostainer was used for the immunohistochemistry with Rat on Mouse-HRP (Biocare Medical) RT517H kit for HSP70 and Bond Polymer Refine Detection (Leica, DS9800) kit for Ki67. Ki-67, a nuclear DNA binding protein which is expressed in all the vertebrates is a widely used marker of proliferation used for grading tumors<sup>13</sup>. Numerous reports from the cell cycle analysis in the nuclei have shown the presence of Ki-67 in the G1, S and G2 phases of the cell cycle and not in the quiescent or resting cells G0 phase suggesting the role of this protein as cell proliferation marker in many cancers<sup>14</sup>. Ki-67 labelling index as determined by immunohistochemistry (IHC) analysis on paraffin embedded section and percent positive frequency is indicative of patient outcomes. Therefore, High Ki-67 index generally shows poor prognosis in clinical conditions<sup>15</sup>. HSP70 is a highly conserved protein that plays a role in response to a variety of stresses, such as aging, metabolic challenge, oxidative stress, and hyperthermia<sup>16</sup>. During hyperthermia treatments, the energy absorption in the tumor causes cell stress and causes the expression of cell stress-associated molecules. One of the most abundant stress-induced molecules is Hsp70, which becomes strongly expressed in response to heat stress and damage<sup>17</sup>. Hsp70 has ambivalent effects on tumor progression as it can mediate both tumor-promoting and tumor-suppressing pathways, depending on its macroscopic (tumor cells or tumor stroma) and microscopic (intracellular or extracellular) localization<sup>18</sup>.

### Statistical analysis

In order to compare the effect on the local tumor control of the combined RT and HT treatment, with respect to RT alone, the Mann-Whitney test was performed at different time points. More precisely statistical analysis was carried out on tumor volume measurements and optical BLI data.

### Data availability

The datasets used and/or analysed during the current study available from the corresponding author on reasonable request.

Received: 2 July 2024; Accepted: 21 August 2024

Published online: 27 August 2024

### References

- Thakkar, J. P. *et al.* Epidemiologic and molecular prognostic review of glioblastoma. *Cancer Epidemiol. Biomark. Prev.* **23**, 1985–1996 (2014).
- Peeken, J. C., Vaupel, P. & Combs, S. E. Integrating hyperthermia into modern radiation oncology: What evidence is necessary?. *Front. Oncol.* **7**, 132 (2017).
- Horsman, M. R. & Overgaard, J. Hyperthermia: A potent enhancer of radiotherapy. *Clin. Oncol. (R. Coll. Radiol.)* **19**, 418–426 (2007).
- Sapareto, S. A. & Dewey, W. C. Thermal dose determination in cancer therapy. *Int. J. Radiat. Oncol. Biol. Phys.* **10**, 787–800 (1984).
- Frazier, N. & Ghandehari, H. Hyperthermia approaches for enhanced delivery of nanomedicines to solid tumors. *Biotechnol. Bioeng.* **112**, 1967–1983 (2015).
- Dickerson, E. B. *et al.* Gold nanorod assisted near-infrared plasmonic photothermal therapy (PPTT) of squamous cell carcinoma in mice. *Cancer Lett.* **269**, 57–66 (2008).
- van Rhoon, G. C., Paulides, M. M., Drizdal, T., Neufeld, E. & Levendag, P. C. Clinical hyperthermia by microwaves: Controlling and improving quality through treatment planning. In *2012 6th European Conference on Antennas and Propagation (EUCAP)*, 1791–1795. <https://doi.org/10.1109/EuCAP.2012.6206702> (2012).
- Ivory, A. M., De Melo Baesso, R., Durando, G., Rajagopal, S. & Miloro, P. Development and testing of a system for controlled ultrasound hyperthermia treatment with a phantom device. *IEEE Trans. Ultrason. Ferroelectr. Freq. Control* (2023).
- Danics, L. *et al.* Exhaustion of protective heat shock response induces significant tumor damage by apoptosis after modulated electro-hyperthermia treatment of triple negative breast cancer isografts in mice. *Cancers (Basel)* **12** (2020).
- Glickstein, B., Aronovich, R., Feng, Y. & Ilovitsh, T. Development of an ultrasound guided focused ultrasound system for 3D volumetric low energy nanodroplet-mediated histotripsy. *Sci. Rep.* **12**, 20664 (2022).
- Verhaegen, F., Granton, P. & Tryggestad, E. Small animal radiotherapy research platforms. *Phys. Med. Biol.* **56**, 55–83 (2011).
- van Hoof, S. J., Granton, P. V. & Verhaegen, F. Development and validation of a treatment planning system for small animal radiotherapy: SMART-Plan. *Radiother. Oncol.* **109**, 361–366 (2013).
- Sobecki, M. *et al.* Cell-cycle regulation accounts for variability in Ki-67 expression levels. *Cancer Res.* **77**, 2722–2734 (2017).
- Urruticoechea, A., Smith, I. E. & Dowsett, M. Proliferation marker Ki-67 in early breast cancer. *J. Clin. Oncol.* **23**, 7212–7220 (2005).
- Perou, C. M. *et al.* Distinctive gene expression patterns in human mammary epithelial cells and breast cancers. *Proc. Natl. Acad. Sci. USA* **96**, 9212–9217 (1999).
- Guzhova, I. V. & Margulis, B. A. HSP70-based anti-cancer immunotherapy. *Hum. Vaccin. Immunother.* **12**, 2529–2535 (2016).
- Rosenzweig, R., Nillegoda, N. B., Mayer, M. P. & Bukau, B. The Hsp70 chaperone network. *Nat. Rev. Mol. Cell Biol.* **20**, 665–680 (2019).
- Juhász, K. *et al.* The complex function of hsp70 in metastatic cancer. *Cancers (Basel)* **6**, 42–66 (2013).

### Acknowledgements

The research leading to these results has received funding from: AIRC under IG 2022, ID. 27336, project PI: Antonello E. Spinelli. EURAMET 18HLT06 RaCHY of the EMPIR program cofinanced by the participating states and from the European Union's Horizon 2020 research and innovation program. The authors would like to acknowledge Dr. Rossella Galli for providing the U87 luc+ cell line.

### Author contributions

G.D., F.V. and A.E.S. conceived the experiments, F.S. and G.D. conducted the experiments, A.M.I., R.M.B. and P.M. developed the US HT system, A.E.S. and F.V. analysed the results. All authors reviewed the manuscript.



### Competing interests

The authors declare no competing interests.

### Additional information

**Correspondence** and requests for materials should be addressed to A.E.S.

**Reprints and permissions information** is available at [www.nature.com/reprints](http://www.nature.com/reprints).

**Publisher's note** Springer Nature remains neutral with regard to jurisdictional claims in published maps and institutional affiliations.

**Open Access** This article is licensed under a Creative Commons Attribution-NonCommercial-NoDerivatives 4.0 International License, which permits any non-commercial use, sharing, distribution and reproduction in any medium or format, as long as you give appropriate credit to the original author(s) and the source, provide a link to the Creative Commons licence, and indicate if you modified the licensed material. You do not have permission under this licence to share adapted material derived from this article or parts of it. The images or other third party material in this article are included in the article's Creative Commons licence, unless indicated otherwise in a credit line to the material. If material is not included in the article's Creative Commons licence and your intended use is not permitted by statutory regulation or exceeds the permitted use, you will need to obtain permission directly from the copyright holder. To view a copy of this licence, visit <http://creativecommons.org/licenses/by-nc-nd/4.0/>.

© The Author(s) 2024